Catalysts **2015**, *5*, 1079-1091; doi:10.3390/catal5031079

OPEN ACCESS

catalysts

ISSN 2073-4344

www.mdpi.com/journal/catalysts

Article

Microwave Synthesis of High Activity $FeSe_2$/C Catalyst toward Oxygen Reduction Reaction

Qiaoling Zheng [1], Xuan Cheng [1,2,*] and Hengyi Li [1]

[1] Department of Materials Science and Engineering, College of Materials, Xiamen University, Xiamen 361005, China; E-Mails: 20720131150074@stu.xmu.edu.cn (Q.Z.); henryzxm1986@126.com (H.L.)

[2] Fujian Key Laboratory of Advanced Materials, Xiamen University, Xiamen 361005, China

* Author to whom correspondence should be addressed; E-Mail: xcheng@xmu.edu.cn; Tel.: +86-592-218-5599; Fax: +86-592-218-3937.

Academic Editor: Minhua Shao

Received: 16 May 2015 / Accepted: 23 June 2015 / Published: 30 June 2015

Abstract: The carbon supported iron selenide catalysts ($FeSe_2$/C) were prepared with various selenium to iron ratios (Se/Fe), namely, Se/Fe = 2.0, 2.5, 3.0, 3.5 and 4.0, through facile microwave route by using ferrous oxalate ($FeC_2O_4 \cdot 2H_2O$) and selenium dioxide (SeO_2) as precursors. Accordingly, effects of Se/Fe ratio on the crystal structure, crystallite size, microstructure, surface composition and electrocatalytic activity for oxygen reduction reaction (ORR) of $FeSe_2$/C in an alkaline medium were systematically investigated. The results revealed that all the $FeSe_2$/C catalysts obtained with the Se/Fe ratios of 2.0–4.0 exhibited almost pure orthogonal $FeSe_2$ structure with the estimated mean crystallite sizes of 32.9–36.2 nm. The electrocatalytic activities in potassium hydroxide solutions were higher than those in perchloric acid solutions, and two peak potentials or two plateaus responded to ORR were observed from cyclic voltammograms and polarization curves, respectively. The ORR potentials of 0.781–0.814 V with the electron transfer numbers of 3.3–3.9 at 0.3 V could be achieved as the Se/Fe ratios varied from 2.0 to 4.0. The Fe and Se were presented at the surface of $FeSe_2$/C upon further reduction on $FeSe_2$. The Se/Fe ratios slightly influenced the degree of graphitization in carbon support and the amount of active sites for ORR.

Keywords: fuel cells; oxygen reduction reaction; electrocatalytic activity; iron selenide catalysts

1. Introduction

Alkaline fuel cells have been attracting extensive attention due to their great advantages in cathode dynamics and with the reduction of ohmic polarization [1]. Oxygen reduction reaction (ORR) is an important process in an electrochemical energy conversion and a four-electron reaction is desirable to take place for a given catalyst in order to achieve good electrocatalytic performance. In recent years, the transition metals such as Mn [2], Fe [3,4], Co [5], Ni [6], Cu [7] and the heteroatom dopants B [8], N [9,10], P [11,12], S [13,14], Se [15] have been reported to modify the catalytic properties of various carbon materials including amorphous carbon, carbon nanotubes, and graphene, which arouse a great deal of interest for the research and development of non-noble catalysts.

Chalcogenides are promising for the potential replacement Pt based cathode catalysts because of their good electrocatalytic activity and high selectivity toward ORR in both acidic and basic media. The onset potential of 0.823 V for ORR could be attained in H_2SO_4 solutions with CoSe/C synthesized through microwave assisted routes [16], while the ORR potentials of 0.6–0.7 V and the electron transfer numbers of 3.1 Oxygen reduction reaction 4.0 could be obtained for $CoSe_2$/C prepared with the Se/Co ratios of 2.5–4.0 [17]. In addition, $CoSe_2$ nanoparticles showed a higher ORR activity in KOH than in H_2SO_4 solutions and a higher tolerance to methanol as compared with a commercial 20 wt % Pt/C catalyst [18]. The tetragonal and cubic Cu_2Se nanowires were found to have the four-electron mechanism, while the cubic nanowires were a dual-path mode in KOH solution [7]. Although FeSe and $FeSe_2$ have been reported for the applications in superconductors or magnetic semiconductors [19–21], their ORR activities have not been investigated so far.

In this work, a series of carbon supported $FeSe_2$ nanoparticles were synthesized using the microwave method with different molar ratios of Se/Fe. The crystal phases, microstructures, chemical compositions and electrocatalytic activities of the as-prepared $FeSe_2$/C catalysts were explored by X-ray diffraction (XRD), transmission electron microscopy (TEM), selected area electron diffraction (SAED), Raman spectroscopy, energy dispersive X-ray spectroscopy (EDS), X-ray photoelectron spectroscopy (XPS), cyclic voltammetry and rotating disk electrode (RDE) techniques. The effect of Se/Fe ratio on ORR activity in an alkaline medium is discussed in terms of ORR active site and carbon graphitization.

2. Results and Discussion

Typical powder XRD patterns of $FeSe_2$/C catalysts prepared with different Se/Fe ratios are shown in Figure 1. Compared with the standard lines of orthogonal $FeSe_2$ phase (PDF#65-2570) included in the bottom of Figure 1a, the major characteristic diffraction peaks appeared at $2\theta \approx 35.0°$, 36.4° and 48.4° belonged to (111), (120) and (211) planes, while a pair of twin peaks near 31° and 50° to (101)/(020) and (031)/(130) planes. A closer examination in the range of 25°–50° revealed that the diffraction peak corresponded to (120) shifted to smaller Bragg angles as evident in Figure 1b. Despite this, the formation

of orthogonal $FeSe_2$ structure is strongly indicated. The average crystallite sizes were evaluated using Scherrer equation described below:

$$d = \frac{K\lambda}{\beta \cos\theta} \quad (1)$$

where d is the mean crystallite size; K is a dimensionless shape factor and has a typical value of 0.89, λ is the X-ray wavelength, λ = 0.1546 nm; β is the full width at half maximum (FWHM); θ is the Bragg scattering angle. The results are given in Table 1. Apparently, the Se/Fe ratios did not significantly influence the average crystallite sizes of the as-prepared $FeSe_2$/C catalysts, which ranged 36.2–32.9 nm with Se/Fe ratios of 2.0–4.0. The empirical Se/Fe ratios, also included in Table 1, were roughly evaluated from EDS data and agreed reasonably well with those nominal ones.

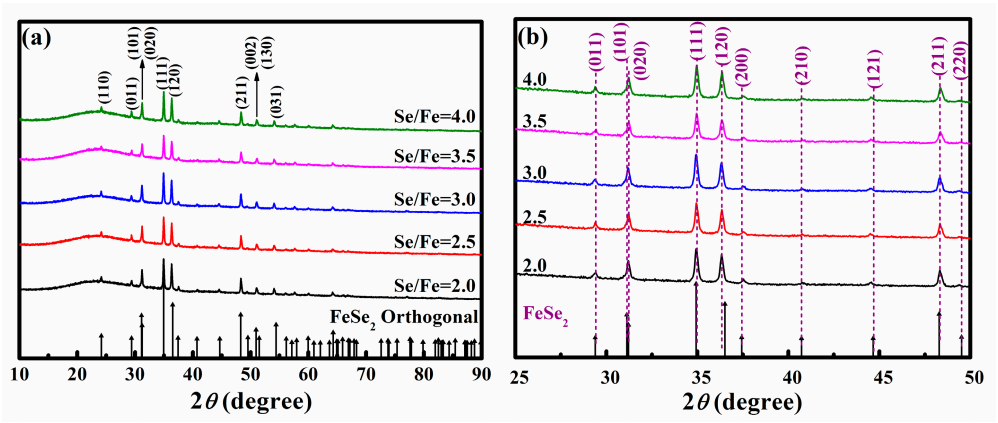

Figure 1. Typical powder XRD patterns of $FeSe_2$/C prepared with different Se/Fe ratios. The standard lines of orthogonal $FeSe_2$ phase are included for comparison. (**a**) Full range in 10°–90°; (**b**) Enlarged in 25°–50°.

Table 1. Parameters of iron selenide catalysts ($FeSe_2$/C) prepared with different Se/Fe ratios.

Parameter		Se/Fe ratio				
Nominal		2.0	2.5	3.0	3.5	4.0
Evaluated by EDS		2.1	2.5	3.3	3.6	4.2
Crystallite Size (nm)		36.2	35.6	32.9	33.1	35.4
E_P (V, *vs.* RHE)	(I)	0.733	0.704	0.733	0.699	0.727
	(II)	0.511	0.514	0.509	0.499	0.478
n at 0.3 V (*vs.* RHE)		3.7	3.9	3.5	3.3	3.6
E_{ORR} (V, *vs.* RHE)		0.814	0.781	0.809	0.795	0.814
I_D/I_G		1.64	1.71	1.76	1.90	1.74
A_{sp}^3/A_{sp}^2		0.37	0.48	0.44	0.51	0.46

The electrocatalytic activities of $FeSe_2$/C prepared with different Se/Fe ratios toward ORR were studied in both acidic and alkaline media. Figure 2 presents the cyclic voltammograms obtained in N_2 (dashed lines) and O_2 (solid lines) saturated 0.1 mol·L^{-1} $HClO_4$ solutions at 50 mV·s^{-1}. No apparent peaks were observed in N_2 atmosphere, while one or two reduction peaks in O_2 atmosphere. Two peak potentials of 0.211 V, −0.045 V and 0.204 V, −0.028 V were obtained only for $FeSe_2$/C prepared with Se/Fe = 2.5 and Se/Fe = 4.0. Obviously, the ORR activity of $FeSe_2$/C in an acidic medium was poor.

The cyclic voltammograms and RDE polarization curves for $FeSe_2$/C prepared with different Se/Fe ratios measured in N_2 (dashed lines) and O_2 (solid lines) saturated 0.1 mol·L^{-1} KOH solutions are illustrated in Figure 3. A large reduction peak I was observed near 0.7 V, and followed by a small reduction peak II around 0.5 V in O_2 saturated KOH solutions (solid lines in Figure 3a). This phenomenon was also observed for vertically aligned carbon nanotubes in a KOH solution [22]. The peak potentials (E_P) could be obtained from Figure 3a and are also summarized in Table 1. The E_P values ranged from 0.699–0.773 V for Peak I and 0.499–0.514 V for Peak II, suggesting an enhanced ORR activity in an alkaline medium. As can be seen in Figure 3b, the plateaus observed for $FeSe_2$/C were not well defined in KOH solutions, which significantly differed from those observed for $CoSe_2$/C in H_2SO_4 solutions [17]. Similarly, the electron transfer numbers (n) of $FeSe_2$/C prepared for different Se/Fe ratios could be determined from the slops of Koutecky-Levich plots at 0.3 V as shown in Figure 4a. The dashed lines indicated the slopes corresponding to two-electron and four-electron reactions. The calculated results are also included in Table 1. The n values varied from 3.3–3.9 at 0.3 V in KOH solutions for $FeSe_2$/C prepared with Se/Fe ratios of 2.0–4.0, while they were 3.1–4.0 in H_2SO_4 solutions for $CoSe_2$/C prepared with Se/Co ratios of 2.0–4.0 [17].

The polarization curves of $FeSe_2$/C prepared with different Se/Fe ratios at 1600 rpm are compared with that of a commercial 20% Pt/C in Figure 4b. The potential at the current density of −0.5 mA·cm^{-2} is defined as E_{ORR} (the inset in Figure 4b) and the values are also provided in Table 1. The E_{ORR} value for 20% Pt/C was 0.992 V, while those for $FeSe_2$/C ranged 0.781–0.814 V with the Se/Fe ratios varying 2.0–4.0. However, two platforms observed with $FeSe_2$/C resulted in slightly larger limiting current densities than 20% Pt/C.

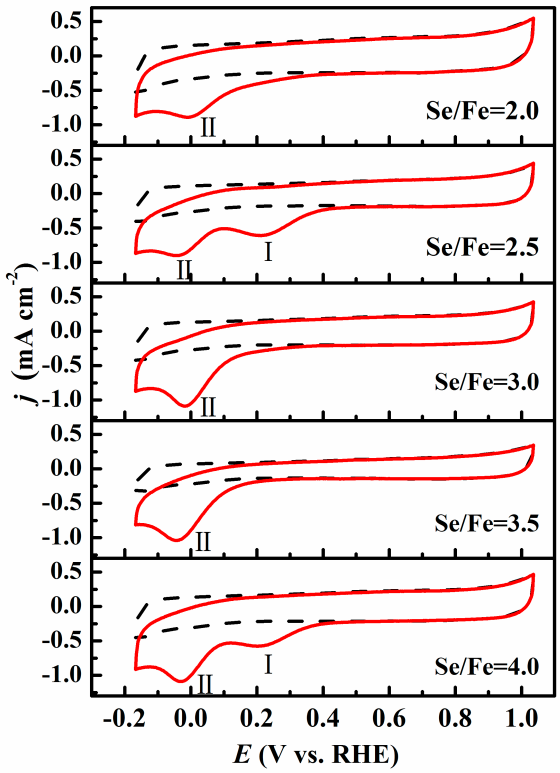

Figure 2. Cyclic voltammograms of $FeSe_2$/C prepared with different Se/Fe ratios in N_2 (dashed lines) and O_2 (solid lines) saturated 0.1 mol·L^{-1} $HClO_4$ solutions at 50 mV·s^{-1}.

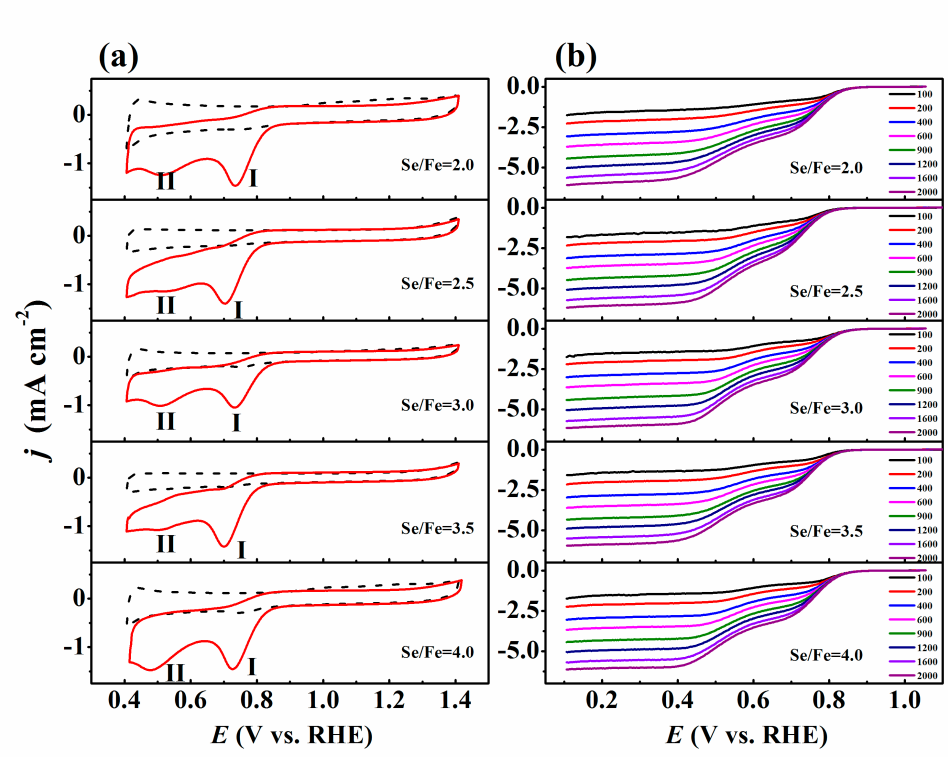

Figure 3. Cyclic voltammograms at 50 mV·s^{-1} (**a**) and RDE polarization curves at 5 mV·s^{-1}; (**b**) of $FeSe_2$/C prepared with different Se/Fe ratios in N_2 (dashed lines) and O_2 (solid lines) saturated 0.1 mol·L^{-1} KOH solutions.

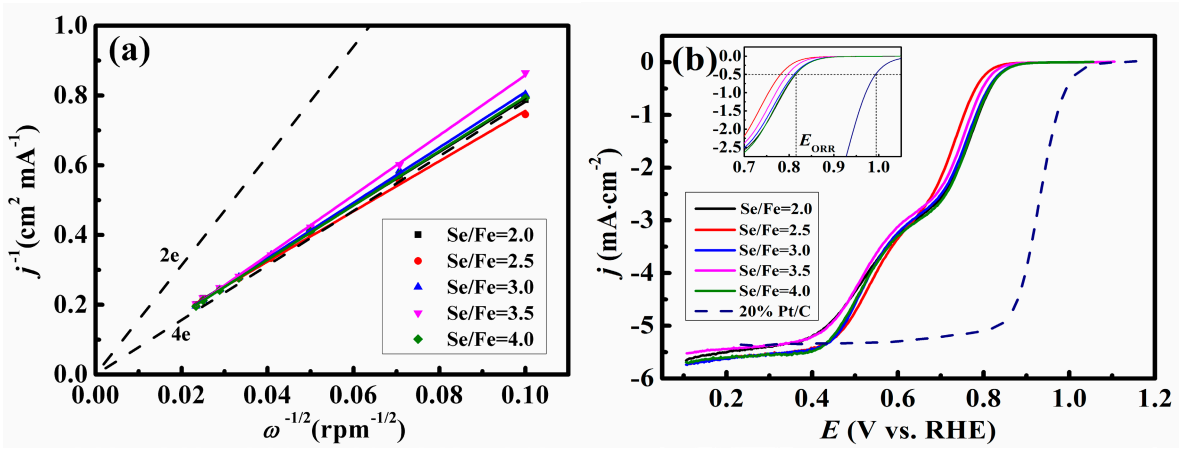

Figure 4. (**a**) Koutecky-Levich plots at 0.3 V; (**b**) RDE polarization curves of Pt/C (dashed line) and $FeSe_2$/C (solid lines) prepared with different Se/Fe ratios in O_2 saturated 0.1 mol·L^{-1} KOH solutions at 1600 rpm. The inset in (**b**) illustrates the potential corresponding to ORR at the current density of −0.5 mA·cm^{-2} (E_{ORR}).

The information in surface species and carbon support could be further studied by obtaining Raman spectra using Ar ion laser excitation of 532 nm as shown in Figure 5. The presences of Fe–Se near 219 cm^{-1}, 284 cm^{-1} and 597 cm^{-1}, as well as Fe–O at 400 cm^{-1} [23,24] are identified in Figure 5a for all the Se/Fe ratios. In Figure 5b, the Raman bands appeared at 1336 cm^{-1} and 1593 cm^{-1} corresponded to D-band of sp^2 type carbon ascribed to the finite-sized crystals of graphite due to the reduction in

symmetry and G-band of all sp^2 bonds in an ideal graphitic layer, respectively. Figure 5c illustrates the curve fitting plots for the Raman data given in Figure 5b. Two additional weak bands at 1191 cm^{-1} and 1499 cm^{-1} belonged to sp^3 type carbon. The relative intensity of the D band over G band (I_D/I_G) and the relative ratio under the areas of sp^3 and sp^2 types of carbon ($A_{sp}{}^3/A_{sp}{}^2$) were calculated, and the results are compared in Table 1. The I_D/I_G and $A_{sp}{}^3/A_{sp}{}^2$ values ranged 1.64–1.90 and 0.37–0.51, respectively, for the Se/Fe ratios of 2.0–4.0. The small difference of I_D/I_G valves might mean that the carbon surface was partially oxygenated without significant structural deformation [25]. The least I_D/I_G and $A_{sp}{}^3/A_{sp}{}^2$ values were obtained for the $FeSe_2$/C prepared with Se/Fe = 2.0, implying the presence of less defect and higher degree graphitization in carbon support. Contrarily, $FeSe_2$/C prepared with Se/Fe = 3.5 showed the largest I_D/I_G and $A_{sp}{}^3/A_{sp}{}^2$ values, and resulted in more defect and lower degree graphitization. Similar I_D/I_G and $A_{sp}{}^3/A_{sp}{}^2$ values were observed for $FeSe_2$/C prepared with Se/Fe = 2.5, 3.0 and 4.0 as evident in Table 1.

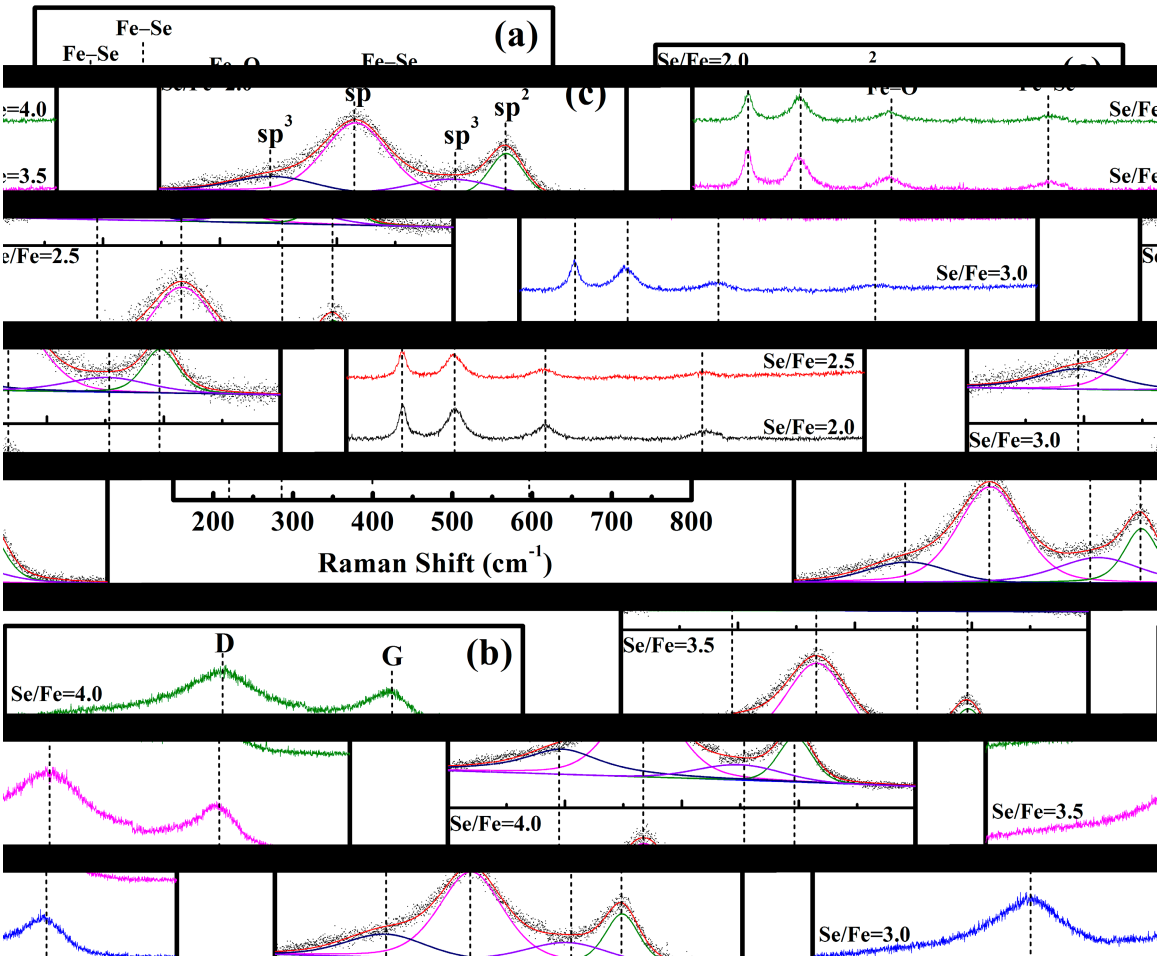

Figure 5. (**a**,**b**) Raman spectra of $FeSe_2$/C prepared with different Se/Fe ratios; (**c**) Fitting curves for Raman spectra (**b**).

The high resolution TEM images and SAED patterns of $FeSe_2$/C prepared with different Se/Fe ratios are supplied in Figures 6 and 7, respectively. The particles sized about 3–12 nm were observed in Figure 6, which are much smaller than those calculated from XRD data (32.9–36.2 nm in T – 1) because XRD gives volume-weighted measurements that tend to overestimate the geometric particle size [26]. The

formation of orthogonal $FeSe_2$ nanoparticles by microwave synthesis was verified by combining both TEM and SAED data, which is consistent with the XRD results in Figure 1.

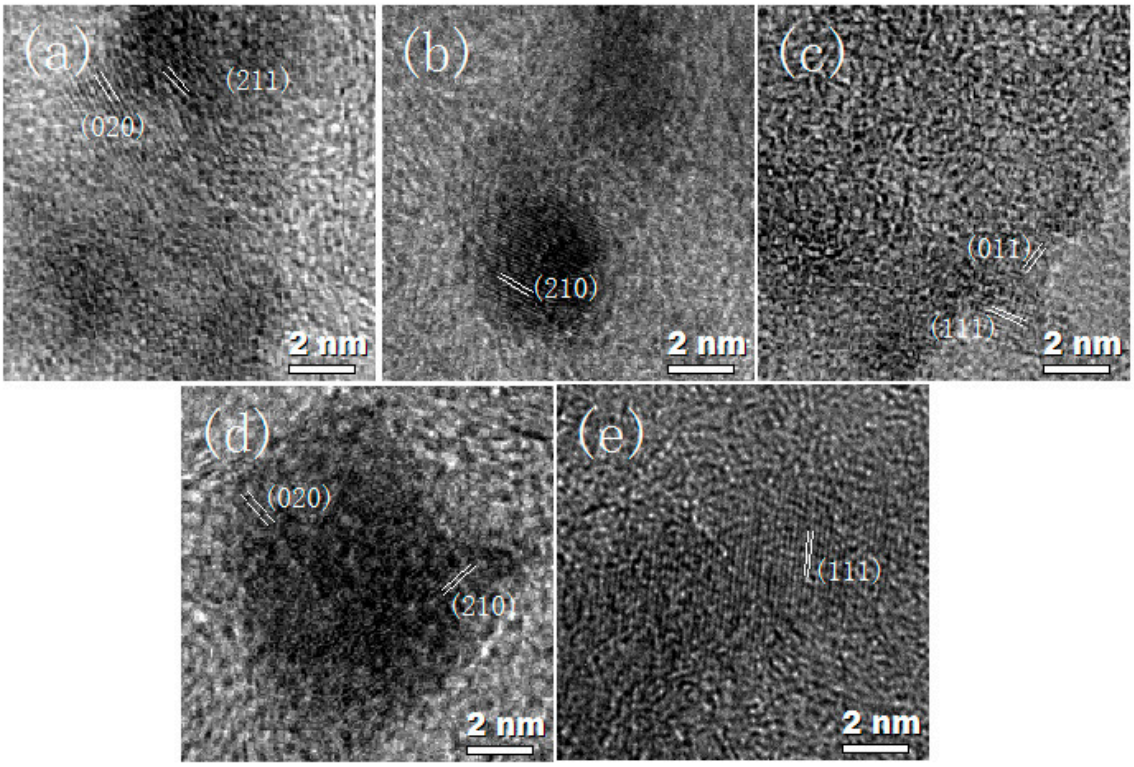

Figure 6. High resolution TEM images of the $FeSe_2$/C prepared with different Se/Fe ratios. (**a**) Se/Fe = 2.0; (**b**) Se/Fe = 2.5; (**c**) Se/Fe = 3.0; (**d**) Se/Fe = 3.5; (**e**) Se/Fe = 4.0.

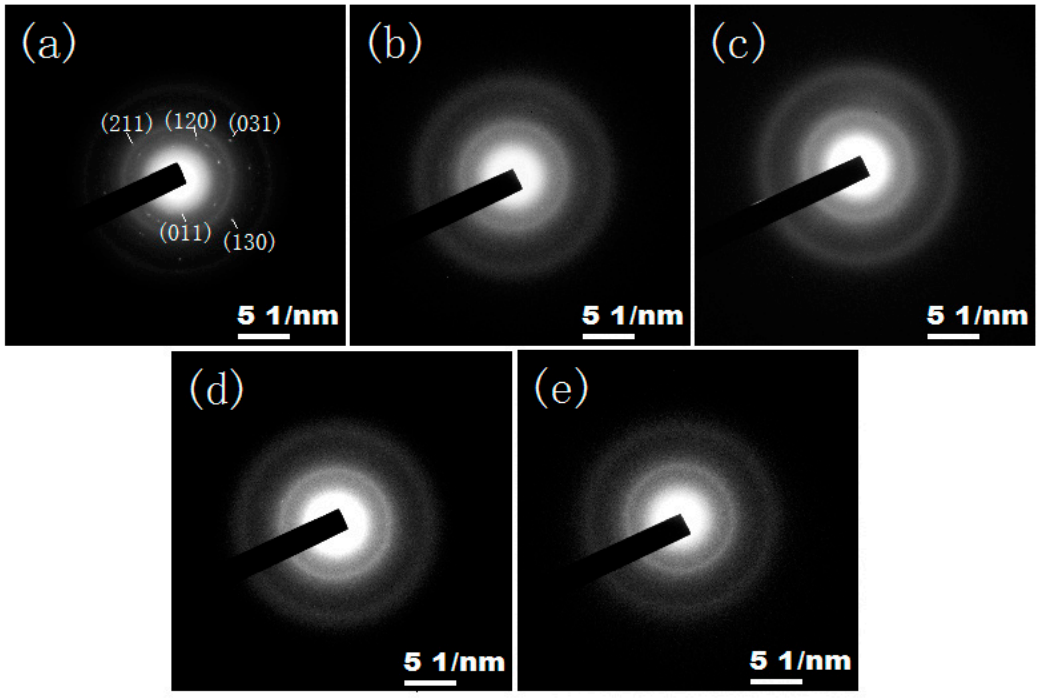

Figure 7. SAED patterns of $FeSe_2$/C prepared with different Se/Fe ratios. (**a**) Se/Fe = 2.0; (**b**) Se/Fe = 2.5; (**c**) Se/Fe = 3.0; (**d**) Se/Fe = 3.5; (**e**) Se/Fe = 4.0.

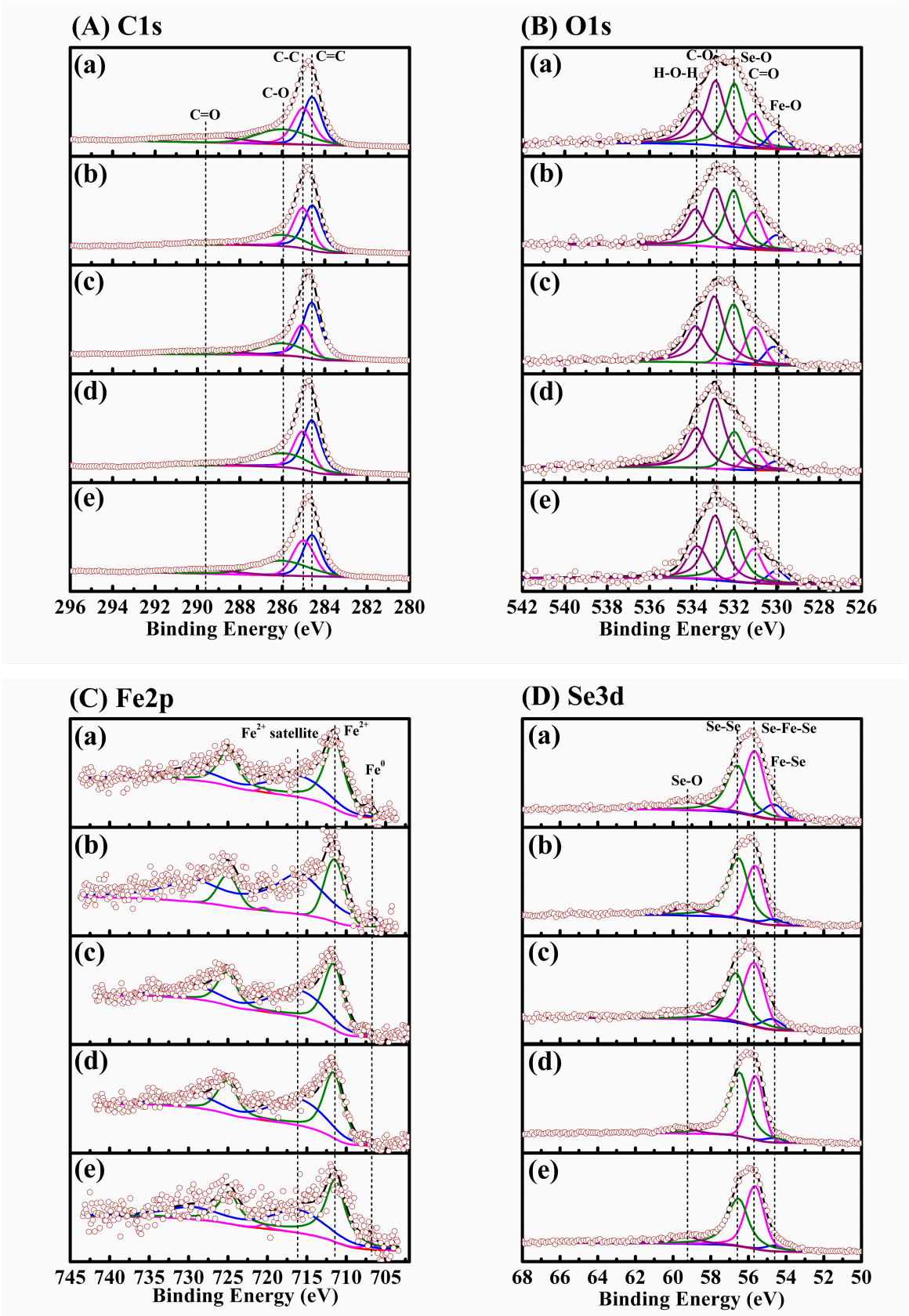

Figure 8. Deconvoluted XPS spectra of (**A**) C1s; (**B**) O1s; (**C**) Fe2p and (**D**) Se3d for $FeSe_2$/C prepared with different Se/Fe ratios. (**a**) Se/Fe = 2.0; (**b**) Se/Fe = 2.5; (**c**) Se/Fe = 3.0; (**d**) Se/Fe = 3.5; (**e**) Se/Fe = 4.0.

Table 2. Surface compositions of $FeSe_2$/C determined based on XPS analyses.

Parameter		Fe/Se ratio									
Nominal		2.0		2.5		3.0		3.5		4.0	
Calculated		2.0		2.5		3.0		3.5		4.0	
Species		E_B (eV)	R.A. (%)	E_B (eV)	R.A. (%).	E_B (eV)	R.A. (%).	E_B (eV)	R.A. (%)	E_B (eV)	R.A. (%)
C1s	C=C	284.6	31.8	284.6	39.8	284.6	47.1	284.6	41.2	284.6	31.3
	C–C	285.0	29.5	285.0	34.3	285.0	22.3	285.0	28.6	285.0	28.7
	C–O	286.0	24.3	286.0	22.4	286.0	21.3	286.0	26.5	286.0	31.0
	C=O	289.6	14.4	289.6	3.5	289.6	9.3	289.6	3.7	289.6	9.0
O1s	Fe–O	530.0	5.9	530.0	6.4	530.1	6.5	530.0	3.7	530.0	5.1
	C=O	531.1	11.2	531.1	13.0	531.1	13.2	531.1	8.3	531.1	15.8
	Se–O	532.0	30.0	532.0	28.2	532.0	20.9	532.0	16.5	532.0	27.9
	C–O	532.9	33.8	532.9	30.6	532.9	37.8	532.9	44.8	532.9	35.5
	H–O–H	533.8	19.0	533.8	21.7	533.8	21.5	533.8	26.6	533.8	15.7
Fe2p	Fe°	707.0	3.7	706.9	3.3	707.0	1.5	707.0	1.4	707.0	5.3
	Fe^{2+}	711.5	96.3	711.5	96.7	711.6	98.5	711.6	98.6	711.4	94.7
	Satellite	716.0	/	715.9	/	716.0	/	716.0	/	716.0	/
Se3d	Fe–Se	54.5	8.8	54.5	5.1	54.6	6.4	54.5	2.7	54.5	4.5
	Se–Fe–Se	55.5	38.4	55.5	32.0	55.6	40.7	55.5	35.5	55.5	43.7
	Se–Se	56.4	38.4	56.4	53.5	56.5	38.5	56.4	57.0	56.4	43.4
	Se–O	59.1	14.3	59.1	9.3	59.1	14.4	59.2	4.8	59.1	8.4

High resolution XPS spectra of C1s, O1s, Fe2p and Se3d were obtained for $FeSe_2$/C prepared with different Se/Fe ratios and are presented in Figure 8. The surface compositions could be evaluated by performing multi-peak fitting analysis of every spectrum, and the deconvoluted XPS spectra are also illustrated in Figure 8. The C1 peaks in Figure 8A were fitted with four components centered at 284.6, 285.0, 286.0 and 290.5 eV, which were attributed to C=C, C–C, C–O and C=O, respectively. The surfaces of carbon support (BP2000) consisted of C=C (sp^2 type) and C–C (sp^3 type) bonding. The origins of C=O and C–O might possibly be from oxygenation of the carbon surface during the preparation [27]. The O1s spectra in Figure 8B were deconvoluted into oxide oxygen species mainly associated with Fe oxide (Fe–O) at 530.0 eV and Se oxide (Se–O) at 532.0 eV, as well as C=O at 531.1 eV, C–O at 532.9 eV, and adsorbed water molecule (H–O–H) at 533.8 eV. The presence of Fe–O was also indicated by Raman spectra in Figure 5a, and the Se–O mainly came from the non-reacted raw material. The Fe2p spectra in Figure 8C suggested the existences of Fe^{2+} related to the formation of major compound of $FeSe_2$ with possible formations of FeSe and Fe oxide (Fe–O). Possible formation of Fe^0 could be resulted from further reduction in $FeSe_2$ (or FeSe) during the microwave preparation. Furthermore, the surface of $FeSe_2$ might become oxidized during the preparation and characterization, which was clearly indicated as Fe–O in Raman spectra (Figure 5a). However, the Fe2p spectra in Figure 8C could not directly differentiated the Fe_3O_4 (Fe^{2+} and Fe^{3+}), Fe_2O_3 (Fe^{3+}) and FeSe, because the binding energies of Fe_3O_4 (711.4 eV), Fe_2O_3 (711.0 eV) and FeSe (711.5 eV) are very close. Similarly, they could not be readily differentiated in O1s based on the binding energy O–Fe–O (530.1 eV) and Fe–O (530.0 eV). The formation of $FeSe_2$ (Se–Fe–Se) could be accompanied by over reduction of $FeSe_2$ since the strong reducing environment was created by using ethylene glycol and glycerol during microwave preparation. Further reduction on $FeSe_2$ occurred for all the Se/Fe ratios at the surface of

$FeSe_2$ and led to formations of FeSe, Fe and Se. In addition, other species such as $FeSe_4$ could also exist for the excess Se, but the exact verification required more detailed study. It has been found that the appropriate excess amounts of SeO_2 could prevent the $CoSe_2$/C nanoparticles from agglomeration and dissolution, which contributed to the improved ORR activity and good stability [17]. The Se3d peaks in Figure 8D indicated the presences of Fe–Se, Se–Fe–Se, Se–Se and Se–O. The relative amounts (R. A.) of surface species could be obtained by multi-peak fitting the XPS data and are summarized in Table 2. The $FeSe_2$ and FeSe were ORR active sites, and the total amounts of $FeSe_2$ and FeSe were 47.2%, 37.1%, 47.1%, 38.2% and 48.2% for Se/Fe = 2.0, 2.5, 3.0, 3.5, and 4.0, respectively, which were consistent with the ORR activities indicated by E_{ORR} values in Table 1. The $FeSe_2$/C catalysts prepared with Se/Fe = 2.5 and Se/Fe = 3.5 showed relatively smaller E_{ORR} values, while those with Se/Fe = 2.0, Se/Fe = 3.0, and Se/Fe = 4.0 had larger E_{ORR} values.

3. Experimental Section

3.1. Materials

The chemical reagents of ferrous oxalate ($FeC_2O_4 \cdot 2H_2O$), selenium dioxide (SeO_2), ethylene glycol and glycerol of analytic grade were purchased from Sinopharm Chemical Reagent Co. Ltd. in China. The carbon support material of Black Pearls 2000 (BP2000) was purchased from Cabot Co. The mean grain size and specific surface area (Brunauer–Emmet–Teller, BET) were 12 nm and 1500 $m^2 \cdot g^{-1}$, respectively.

3.2. Catalyst Synthesis

The amounts of 40.0 mg $FeC_2O_4 \cdot 2H_2O$ were dissolved in 2 mL ethylene glycol and a certain amount of 0.161 mmol/mL SeO_2 aqueous solution with the different molar ratios of Se/Fe, namely, 2.0, 2.5, 3.0, 3.5, 4.0. Then, a certain amount of glycerol was added, and the mixed solution was agitated with a glass rod and homogenized in an ultrasonic bath for 30 min. The BP2000 was continually added during the ultrasonic processing. The loading amount of $FeSe_2$ on carbon was about 36% according to the weight ratio at the start of the feeding. The homogeneous solution was placed in a microwave oven by using 800 W for 180 s while the solution cooled to room temperature, which was sonicated and stirred for 4 h. The product was finally centrifuged, washed with ethanol and deionized water, and dried in a vacuum oven at 338 K for 12 h.

3.3. Electrochemical Characterization

The electrochemical measurements were carried out by using the electrochemical test station (Autolab-PGSTAT30) with rotation disc electrode (RDE) system (Pine Research Instrument) in a conventional three-electrode cell. A glassy carbon RDE was a working electrode, a Pt mesh (2 cm × 2 cm) a counter electrode and a Ag/AgCl a reference electrode. Catalyst ink was prepared by homogeneously dispersing 2 mg of the as-prepared $FeSe_2$/C powder ultrasonically in a solution mixture containing 0.5 mL isopropanol and 10 μL 5 wt. % Nafion solution. Then, 10 μL of the mixture was transferred onto the 0.196 cm^{-2} polished glassy carbon electrode surface and dried at room temperature. The catalyst loadings on the electrodes were evaluated to be 0.2 $mg \cdot cm^{-2}$ (including the support).

The cyclic voltammetry (CV) and RDE measurements were done at 20 °C in either nitrogen purged or oxygen saturated 0.1 mol·L^{-1} $HClO_4$ and 0.1 mol·L^{-1} KOH solutions. Prior to the measurement, the electrolyte was deaerated by nitrogen or oxygen throughout the 30 min. The scanning potentials started from -0.160 V to 1.034 V in $HClO_4$ or 0.413 V to 1.410 V in KOH at a sweep rate of 50 mV·s^{-1}. The linear sweep voltammetry (LSV) curves were recorded in the potential range of 0.107–1.105 V with 5 mV·s^{-1} over a rotation rate of 0–2000 rpm in oxygen saturated electrolyte. All the potentials in this work were reported with respect to reversible hydrogen electrode (RHE).

3.4. Physicochemical Characterization

XRD analysis of the catalyst nanoparticles was performed with a powder diffractometer (Rigaku Ultima IV XRD) using Cu K_α radiation (λ = 0.1546 nm). Raman spectra were acquired using the 532 nm laser on a Princeton TriVista CRS557 Raman spectrometer. A high resolution transmission electron microscope (TEM) (JEOL JEM-2100), field emission scanning electron microscope (SEM) with built-in energy dispersive X-ray spectroscope (EDS) (Zeiss Sigma SEM) and X-ray photoelectron spectroscope (XPS) (PHI Quantum 2000) using Al K_α radiation were used to examine the microstructures and chemical compositions of the as-prepared catalyst nanoparticles, respectively.

4. Conclusions

The $FeSe_2$/C catalysts could be rapidly prepared through a simple microwave method by using various Se/Fe ratios. The formation of the orthogonal $FeSe_2$ structure was confirmed by XRD, TEM and SAED analyses. The estimated average crystallite sizes were 32.9–36.2 nm for the Se/Fe ratios of 2.0–4.0. The catalysts exhibited the enhanced ORR activities in alkaline media rather than in acidic media. The ORR potentials of 0.781–0.814 V with the electron transfer numbers of 3.3–3.9 at 0.3 V could be achieved in KOH solutions as the Se/Fe ratios varied from 2.0 to 4.0. The Se/Fe ratios slightly influenced the amounts of ORR active sites and the defects of carbon support, as well as the degrees of graphitization, which together affected the ORR activities.

Acknowledgments

The authors wish to thank the financial support provided by the National Natural Science Foundation of China (11372263).

Author Contributions

Q.Z. prepared the samples and performed all the measurements; X.C. prepared the manuscript; H.L. assisted for experimental design.

Conflicts of Interest

The authors declare no conflict of interest.

References

1. McLean, G.; Niet, T.; Prince-Richard, S.; Djilali, N. An assessment of alkaline fuel cell technology. *Int. J. Hydrogen Energy* **2002**, *27*, 507–526.
2. Liang, Y.; Wang, H.; Zhou, J.; Li, Y.; Wang, J.; Regier, T.; Dai, H. Covalent hybrid of spinel manganese–cobalt oxide and graphene as advanced oxygen reduction electrocatalysts. *J. Am. Chem. Soc.* **2012**, *134*, 3517–3523.
3. Lefèvre, M.; Proietti, E.; Jaouen, F.; Dodelet, J.P. Iron-based catalysts with improved oxygen reduction activity in polymer electrolyte fuel cells. *Science* **2009**, *324*,71–74.
4. Cao, R.; Thapa, R.; Kim, H.; Xu, X.; Kim, M.G.; Li, Q.; Park, N.; Liu, M.; Cho, J. Promotion of oxygen reduction by a bio-inspired tethered iron phthalocyanine carbon nanotube-based catalyst. *Nat. Commun.***2013**, *4*, 2076.
5. Shin, D.; Jeong, B.; Mun, B.S.; Jeon, H.; Shin H.J.; Baik, J.; Lee, J. On the Origin of Electrocatalytic Oxygen Reduction Reaction on Electrospun Nitrogen–Carbon Species. *J. Phys. Chem. C* **2013**, *117*, 11619–11624.
6. Ding, L.; Xin, Q.; Zhou, X.; Qiao, J.; Li, H.; Wang, H. Electrochemical behavior of nanostructured nickel phthalocyanine (NiPc/C) for oxygen reduction reaction in alkaline media. *J. Appl. Electrochem.* **2013**, *43*, 43–51.
7. Liu, S.; Zhang, Z.; Bao, J.; Lan, Y.; Tu, W.; Han, M.; Dai, Z. Controllable Synthesis of Tetragonal and Cubic Phase Cu_2Se Nanowires Assembled by Small Nanocubes and Their Electrocatalytic Performance for Oxygen Reduction Reaction. *J. Phys. Chem. C* **2013**, *117*, 15164–15173.
8. Yang, L.; Jiang, S.; Zhao, Y.; Zhu, L.; Chen, S.; Wang, X.; Wu, Q.; Ma, J.; Ma, Y.; Hu, Z. Boron-Doped Carbon Nanotubes as Metal-Free Electrocatalysts for the Oxygen Reduction Reaction. *Angew. Chem.* **2011**, *123*, 7270–7273.
9. Gong, K.; Du, F.; Xia, Z.; Durstock, M.; Dai, L. Nitrogen-doped carbon nanotube arrays with high electrocatalytic activity for oxygen reduction. *Science* **2009**, *323*, 760–764.
10. Hibino, T.; Kobayashi, K.; Heo, P. Oxygen reduction reaction over nitrogen-doped graphene oxide cathodes in acid and alkaline fuel cells at intermediate temperatures. *Electrochim. Acta* **2013**, *112*, 82–89.
11. Wu, J.; Yang, Z.; Li, X.; Sun, Q.; Jin, C.; Strasser, P.; Yang, R. Phosphorus-doped porous carbons as efficient electrocatalysts for oxygen reduction. *J. Mater. Chem. A* **2013**, *1*, 9889–9896.
12. Zhu, J.; He, G.; Liang, L.; Wan, Q.; Shen, P.K. Direct anchoring of platinum nanoparticles on nitrogen and phosphorus-dual-doped carbon nanotube arrays for oxygen reduction reaction. *Electrochim. Acta* **2015**, *158*, 374–382.
13. Liang, J.; Jiao, Y.; Jaroniec, M.; Qiao, S.Z. Sulfur and Nitrogen Dual-Doped Mesoporous Graphene Electrocatalyst for Oxygen Reduction with Synergistically Enhanced Performance. *Angew. Chem. Int. Ed.* **2012**, *51*, 11496–11500.
14. Susac, D.; Zhu, L.; Teo, M.; Sode, A.; Wong, K.C.; Wong, P.C.; Parsons, R.R.; Bizzotto, D.; Mitchell, K.A.R; Campbell, S.A. Characterization of FeS_2-based thin films as model catalysts for the oxygen reduction reaction. *J. Phys. Chem. C* **2007**, *111*, 18715–18723.

15. Jin, Z.; Nie, H.; Yang, Z.; Zhang, J.; Liu, Z.; Xu, X.; Huang, S. Metal-free selenium doped carbon nanotube/graphene networks as a synergistically improved cathode catalyst for oxygen reduction reaction. *Nanoscale* **2012**, *4*, 6455–6460.
16. Nekooi, P.; Akbari, M.; Amini, M.K. CoSe nanoparticles prepared by the microwave-assisted polyol method as an alcohol and formic acid tolerant oxygen reduction catalyst. *Int. J. Hydrogen Energy* **2010**, *35*, 6392–6398.
17. Li, H.; Gao, D.; Cheng, X. Simple microwave preparation of high activity Se-rich $CoSe_2$/C for oxygen reduction reaction. *Electrochim. Acta* **2014**, *138*, 232–239.
18. Feng, Y.; Alonso-Vante, N. Carbon-supported cubic $CoSe_2$ catalysts for oxygen reduction reaction in alkaline medium. *Electrochim. Acta* **2012**, *72*, 129–133.
19. Oyler, K.D.; Ke, X.; Sines, I.T.; Schiffer, P.; Schaak, R.E. Chemical Synthesis of Two-Dimensional Iron Chalcogenide Nanosheets: FeSe, FeTe, Fe (Se, Te), and $FeTe_2$. *Chem. Mater.* **2009**, *21*, 3655–3661.
20. Han, D.S.; Batchelor, B.; Abdel-Wahab, A. Sorption of selenium (IV) and selenium (VI) onto synthetic pyrite (FeS_2): Spectroscopic and microscopic analyses. *J. Colloid Interface Sci.* **2012**, *368*, 496–504.
21. Burrard-Lucas, M.; Free, D.G.; Sedlmaier, S.J.; Wright, J.D.; Cassidy, S.J.; Hara, Y.; Corkett, A.J.; Lancaster, T.; Baker, P.J.; Blundell, S.J. Enhancement of the superconducting transition temperature of FeSe by intercalation of a molecular spacer layer. *Nat. Mater.* **2013**, *12*, 15–19.
22. Wang, S.; Iyyamperumal, E.; Roy, A.; Xue, Y.; Yu, D.; Dai, L. Vertically Aligned BCN Nanotubes as Efficient Metal-Free Electrocatalysts for the Oxygen Reduction Reaction: A Synergetic Effect by Co-Doping with Boron and Nitrogen. *Angew. Chem. Int. Ed.* **2011**, *50*, 11756–11760.
23. Campos, C.; de Lima, J.; Grandi, T.; Machado, K.; Pizani, P. Structural studies of iron selenides prepared by mechanical alloying. *Solid State Commun.* **2002**, *123*, 179–184.
24. Frost, R.L.; Xi ,Y.; López, A.; Scholz, R.; de Carvalho Lana, C.; e Souza, B.F. Vibrational spectroscopic characterization of the phosphate mineral barbosalite $Fe^{2+}Fe^{3+}_2(PO_4)_2(OH)_2$ – Implications for the molecular structure. *J. Mol. Struct.* **2013**, *1051*, 292–298.
25. Hibino, T.; Kobayashi, K.; Nagao, M.; Kawasaki, S. High-temperature supercapacitor with a proton-conducting metal pyrophosphate electrolyte. *Sci. Rep.* **2015**, *5*, 7903.
26. Warren, B.E. *X-ray Diffraction*; Dover Publications: Mineola, NY, USA, 1969, Volume II, pp. 251-257.
27. Kobayashi, K.; Nagao, M.; Yamamoto, Y.; Heo, P.; Hibino T. Rechargeable PEM fuel-cell batteries using porous carbon modified with carbonyl groups as anode materials. *J. Electrochem. Soc.* **2015**, *162*, F868–F877.